Cellular/Molecular

Single I_h Channels in Pyramidal Neuron Dendrites: Properties, Distribution, and Impact on Action Potential Output

Maarten H. P. Kole,[1]* Stefan Hallermann,[2]* and Greg J. Stuart[1]

[1]Division of Neuroscience, John Curtin School of Medical Research, Australian National University, Canberra 0200, Australian Capital Territory, Australia, and [2]Physiologisches Institut I, Universität Freiburg, D-79104 Freiburg, Germany

The hyperpolarization-activated cation current (I_h) plays an important role in regulating neuronal excitability, yet its native single-channel properties in the brain are essentially unknown. Here we use variance-mean analysis to study the properties of single I_h channels in the apical dendrites of cortical layer 5 pyramidal neurons *in vitro*. In these neurons, we find that I_h channels have an average unitary conductance of 680 ± 30 fS ($n = 18$). Spectral analysis of simulated and native I_h channels showed that there is little or no channel flicker below 5 kHz. In contrast to the uniformly distributed single-channel conductance, I_h channel number increases exponentially with distance, reaching densities as high as ~550 channels/μm^2 at distal dendritic sites. These high channel densities generate significant membrane voltage noise. By incorporating a stochastic model of I_h single-channel gating into a morphologically realistic model of a layer 5 neuron, we show that this channel noise is higher in distal dendritic compartments and increased threefold with a 10-fold increased single-channel conductance (6.8 pS) but constant I_h current density. In addition, we demonstrate that voltage fluctuations attributable to stochastic I_h channel gating impact on action potential output, with greater spike-timing precision in models with the experimentally determined single-channel conductance. These data suggest that, in the face of high current densities, the small single-channel conductance of I_h is critical for maintaining the fidelity of action potential output.

Key words: **HCN; nonstationary fluctuation analysis; spike timing; noise; cortex; gain**

Introduction

Nonselective hyperpolarization-activated currents in the heart (I_f) (Brown et al., 1979) and brain (I_h) (Halliwell and Adams, 1982) are crucial for a wide range of physiological processes, including rhythmogenesis, dendritic excitability, and synaptic transmission (Santoro and Tibbs, 1999; Robinson and Siegelbaum, 2003). These diverse functional roles are dependent, in part, on the elementary single-channel properties underlying I_f and I_h. At the molecular level, I_f and I_h are encoded by four distinct channel isoforms, called hyperpolarization-activated cyclic nucleotide-gated channels (HCN1–HCN4) (Ludwig et al., 1998; Santoro et al., 1998; Biel et al., 2002), each consisting of six membrane-spanning domains centered around a pore with a C terminus containing a cyclic nucleotide binding site (Santoro and Tibbs, 1999; Wainger et al., 2001; Zagotta et al., 2003). Whereas the first single-channel recordings of I_f in dissociated cardiac cells indicated a small unitary conductance of 0.98 pS (DiFrancesco, 1986), recent recordings of I_h in acutely dissociated CA1 neurons reported a 10-fold larger single-channel conductance of 10 pS (Simeone et al., 2005). Conflicting observations of HCN single-channel conductance have also been reported for heterologously expressed HCN subunits, with values of the HCN2 unitary conductance ranging from 2.5 pS (Johnson and Zagotta, 2005) to ~35 pS (Michels et al., 2005).

In this study, we aimed to resolve the unitary properties of single I_h channels in the brain in intact preparations (brain slices) using nonstationary fluctuation analysis (NSFA) (Sigworth, 1980) of macroscopic I_h currents recorded in cell-attached patches from the dendrites of cortical layer 5 pyramidal neurons. In these neurons, I_h is nonuniformly distributed with a significantly higher current density in the distal apical dendrites (Stuart and Spruston, 1998; Williams and Stuart, 2000; Berger et al., 2001; Lorincz et al., 2002; Notomi and Shigemoto, 2004), where it acts to shorten the duration of local dendritic postsynaptic events, diminishing distance-dependent effects on somatic EPSP and IPSP time course as well as temporal summation (Magee, 1998; Stuart and Spruston, 1998; Williams and Stuart, 2000, 2003; Berger et al., 2001).

Our observations indicate that I_h channels have a small unitary conductance of ~0.68 pS, which is uniform along the somatodendritic axis. Furthermore, we find that an exponential increase in single-channel number underlies the nonuniform spatial distribution of I_h, and show that stochastic gating of I_h

Received Aug. 30, 2005; revised Dec. 21, 2005; accepted Dec. 21, 2005.

This work was supported by the Alexander von Humboldt Foundation (G.J.S.) and the Förderkreis of the German Primate Center (Göttingen, Germany) (M.H.P.K.). We are grateful to M. Heckmann for critical reading of previous versions of this manuscript.

*M.H.P.K. and S.H. contributed equally to this work.

Correspondence should be addressed to Maarten H. P. Kole at the above address. E-mail: maarten.kole@anu.edu.au.

DOI:10.1523/JNEUROSCI.3664-05.2006

 0270-6474/06/261677-11$15.00/0

channels leads to significant voltage membrane noise. Finally, we demonstrate using simulations that fluctuations in membrane potential attributable to I_h channel gating are sufficiently large to influence action potential (AP) fidelity in response to synaptic or weak periodic perithreshold inputs.

Materials and Methods

Patch-clamp recordings. Male Wistar rats (28–70 d) were deeply anesthetized by halothane inhalation. After decapitation, the brain was quickly removed, and sagittal brain slices (300 μm) of somatosensory cortex were prepared according to guidelines approved by the Animal Ethics Committee of the Australian National University. Throughout the preparation of slices, the brain was maintained in ice-cold artificial CSF (ACSF) of the following composition (in mM): 125 NaCl, 25 $NaHCO_3$, 3 KCl, 1.25 NaH_2PO_4, 25 glucose, 0.5 $CaCl_2$, and 6 $MgCl_2$, pH 7.4 (95% O_2/5% CO_2). After cutting, slices were transferred to a holding chamber filled with the same ACSF maintained at 35°C for 45 min and subsequently stored at room temperature.

Individual slices were transferred to the stage of an upright microscope (BX51WI; Olympus Optical, Tokyo, Japan) equipped with differential interference contrast (DIC) optics, and the apical dendrites of layer 5 pyramidal neurons were visualized under infrared (IR) light (Stuart and Sakmann, 1994). The recording chamber was perfused with oxygenated (95% O_2/5% CO_2) ACSF consisting of the following (in mM): 125 NaCl, 25 $NaHCO_3$, 3 KCl, 1.25 NaH_2PO_4, 25 glucose, 2 $CaCl_2$, and 1 $MgCl_2$. Somatic and dendritic cell-attached recordings were performed with borosilicate glass pipettes (Harvard Apparatus, Edenbridge, Kent, UK) pulled to a uniform resistance of ~10 MΩ, and filled with the following solution (in mM): 120 KCl, 20 tetraethylammonium-Cl, 10 HEPES, 5 EGTA, 5 4-AP, 1 $MgCl_2$, 1 or 3 $BaCl_2$, 1 $NiCl_2$, 0.5 $CdCl_2$, and 0.001 TTX, pH 7.4 (285 mOsm). For NSFA, a high concentration of $BaCl_2$ (3 mM) was included to block large-conductance channel openings of inward-rectifying K^+ channels. Somatic and dendritic whole-cell recordings were made with pipettes containing 135 mM K-gluconate, 7 mM NaCl, 2 mM $MgCl_2$, 2 mM Na_2ATP, 0.3 mM NaGTP, 10 mM HEPES, pH 7.2 with KOH, and 0.2% biocytin (Invitrogen, Carlsbad, CA). All data were obtained at 34 ± 1°C.

Currents were recorded with an Axopatch 200B amplifier (Molecular Devices, Union City, CA) in capacitive feedback mode and collected using an ITC-18 computer interface (InstruTech, Port Washington, NY). All signals were analog low-pass filtered at 10 kHz (eight-pole Bessel) and digitally sampled at 20 kHz using the data acquisition software Axograph (Molecular Devices). Ensemble traces were further digitally filtered at the indicated frequencies (see below). Baseline recording noise was ~600 fA root mean square (rms) at 5 kHz bandwidth and 1.0 pA at 10 kHz. The bath level of the recording chamber was kept to a minimum to reduce fast capacitance transients. Remaining transients were cancelled with capacitance compensation. Leak subtraction was generally performed off-line using scaled and averaged leak pulses (50 repetitions) using a P/10 protocol.

Voltage signals were recorded with a BVC-700 current-clamp amplifier (Dagan, Minneapolis, MN), filtered at 1 kHz, and sampled at 2 kHz. Capacitance transients and access resistance were compensated with the amplifier circuits. The instrumental noise from the electrode-amplifier circuit was estimated to be ~40 μV by replacing the electrode holder with a model cell (500 MΩ/33 pF; Molecular Devices). Synaptic conductances were blocked by bath application of 50 μM D-APV, 20 μM DNQX, and 50 μM bicuculline-methobromide, and Na^+ channels were blocked with 1 μM TTX (Tocris Bioscience, Bristol, UK). To investigate the impact of I_h channel gating on voltage noise, we bath applied the I_h antagonist ZD 7288 [4-(*N*-ethyl-*N*-phenylamino)-1,2-dimethyl-6-(methylamino) pyrimidinium chloride] in recordings in which somatic noise was >100 μV. Cells with large spontaneous fluctuations in resting potential were disregarded from analysis. Some neurons (see Fig. 1*A*) were processed for biocytin and reconstructed *post hoc* with Neurolucida (MicroBrightField, Williston, VT).

Data analysis. The patch holding potential was calculated assuming a resting potential at the soma of −79 mV, estimated from perforated-patch recordings (Gulledge and Stuart, 2003). In addition, we corrected for a distance-dependent depolarization of the membrane potential of ~1 mV/100 μm (supplemental Fig. S1, available at www.jneurosci.org as supplemental material) and a liquid junction potential of the cell-attached solution of −3 mV (Williams and Stuart, 2000). Somatic whole-cell voltage was corrected for the −14 mV difference between the resting membrane potential during perforated-patch and whole-cell recordings (Gulledge and Stuart, 2003), primarily attributable to the liquid junction potential of the whole-cell pipette solution (−12 mV). The distance of the dendritic recording site from the soma was measured *in situ* from the IR-DIC image and taken to be the linear distance between the recording site and the beginning of the apical trunk.

Steady-state activation curves (see Fig. 1*C*) were constructed from the amplitude of tail currents after voltage steps to different amplitudes (Williams and Stuart, 2000). These data were normalized to the maximum tail current amplitude and fitted with a single Boltzmann function. Activation time course of I_h onset was described by double-exponentials fits from which an amplitude weighed single exponential, $\tau_w = (A\tau_{fast} + B\tau_{slow})/(A + B)$, was calculated. The deactivation time course was well described by a single-exponential function. Average values are expressed as mean ± SEM.

Nonstationary fluctuation analysis. NSFA of recorded, as well as simulated, I_h currents was performed according to recently described routines for voltage-dependent channels (Conti et al., 1980; Sigworth, 1980; Alvarez et al., 2002) written in and analyzed with Igor Pro 5.01 (WaveMetrics, Lake Oswego, OR). In brief, assuming that the macroscopic ionic current at a given time point (t) is dependent on the single-channel properties, such that $I(t) = N\gamma P_o(V,t)\,(V - V_{REV})$, where I is the current, and V the membrane voltage. The current is the product of N, the maximum number of channels, γ, the elementary single-channel conductance, P_o, the probability of channel opening at maximum steady-state current, and the electrical driving force, $V - V_{REV}$, where V_{REV} is the reversal potential.

The variance, σ_I^2, in trial-to-trial fluctuations of the ensemble I_h current evoked by identical hyperpolarizing steps (−60 or −100 mV; 400 ms duration) was calculated from sets of 80–140 consecutive sweeps. To correct for rundown of the ensemble I_h current, we followed procedures described previously (Conti et al., 1980; Alvarez et al., 2002). The variance was defined by:

$$\sigma_I^2(t) = \frac{2}{N_{tr} - 1} \sum_{i=1}^{N_{tr}} (y_i(t) - \bar{y}(t))^2$$

$$\text{with } y_i(t) = \frac{x_i(t) - x_{i+1}(t)}{2},$$

where N_{tr} is the number of evaluated traces (in most cases, 100), $x_i(t)$ are the values of the ith current trace, and $\bar{y}$ is the average of all y_i. Variance-mean plots were fitted with a least-square algorithm to the following equation:

$$\sigma_I^2 = i\langle I\rangle - \frac{\langle I\rangle^2}{N} + B.$$

Here, B is a background noise offset, and $\langle I\rangle$ is the mean current. At the first root of the parabola, the slope equals the single-channel amplitude i. Variance-mean plots were calculated from data beginning 2 ms after the start of the voltage pulse to the maximum of the steady-state mean amplitude. Single-channel conductance, γ, was estimated by $i/(V - V_{REV})$, and the open probability, P_o, was determined by $P_o = I_{max}/(iN)$, where I_{max} is the average current amplitude at steady state. The reversal potential (V_{REV}) was experimentally measured to be ~0 mV (0.5 ± 2.6 mV; $n = 4$) with 120 mM external K^+ and zero Na^+. For 60 mM external K^+ and Na^+, and 2.5 mM external K^+ and 120 mM external Na^+, we calculated a V_{REV} of −16 and −45 mV, respectively, based on the Goldman–Hodgkin–Katz equation assuming an Na^+ to K^+ permeability ratio of 0.4 and 0.2 (Hestrin, 1987). Similar values of N, i, or P_o were obtained during NSFA of the first 200 ms ($n = 18$; $p > 0.3$) and also after exponential sampling ($n = 18$; $p > 0.7$), where mean current and variance were sampled in an exponentially manner based on τ_w.

I_h current simulations. Single I_h channel currents in the models shown in Figure 2 were simulated at 20 kHz temporal resolution (identical to the sampling frequency of recordings) with the high quality pseudorandom number generator in Igor Pro [compare with function ran2 by Press (2002)]. The uniformly distributed number, u, between 0 and 1 was used to generate an exponentially distributed interval $-(1/a) \times ln(u)$, where a is the sum of the rate constants from one state to all neighboring states. Another random number was used to decide which state was visited next (Colquhoun et al., 2003). Simulated macroscopic I_h currents, with activation kinetics similar to the weighed activation time constant of experimental data ($\tau_w = 50$ ms), were generated by the addition of the appropriate number of single-channel currents. Realistic recording noise (1 pA rms at 10 kHz) was simulated by adding white noise (simulated with Igor Pro; Box-Müller transformation) with 1.22 pA rms to each point. Filtering with a low-pass Gaussian filter with a cutoff frequency of 10 kHz resulted in 1 pA rms, similar to that observed in patch-clamp recordings after low-pass filtering at 10 kHz using the eight-pole Bessel filter of the amplifier. As in the experimental situation, we repeated this procedure 100 times. The resulting 100 simulated macroscopic currents were analyzed with NSFA identical to the recorded data. Leak subtraction was implemented by subtracting a simulated empty leak current (an average of 50 traces of 1 pA rms noise scaled up by a factor of 10) from the mean current.

NEURON simulations. The impact of I_h channel fluctuations on AP output was simulated using a morphological realistic compartmental model of a large layer 5 pyramidal neuron (Stuart and Spruston, 1998, their Fig. 1*A*) in NEURON (version 5.7, available at http://www.neuron.yale.edu/neuron/). Spines were incorporated by decreasing R_m and increasing C_m twofold in spiny compartments. The passive properties R_m (15 kΩ/cm^2), C_m (1 μF/cm^{-2}), and R_i (100 Ω/cm) were uniformly distributed, and the resting membrane potential V_m was set at -89 mV, equivalent to the experimentally recorded V_m when I_h was blocked with 50 μM ZD 7288. To account for active properties, voltage-gated channels (Schaefer et al., 2003) were incorporated at the following densities. The soma contained (in pS/μm^2) $g_{Na} = 54$, $g_{Kv} = 200$, $g_{KaP} = 0.008$, $g_{Kca} = 3$, $g_{Km} = 0.1$, calcium $g_{Ca} = 0.3$, and $g_{Ca,T} = 0.0008$. In the dendrites the channel densities were as follows: $g_{Na} = 27$, $g_{Kv} = 25$, $g_{KaP} = 0.008$, $g_{Kca} = 1.5$, $g_{Km} = 0.05$, $g_{Ca} = 0.8$, and $g_{Ca,T} = 0.0005$. In the reconstructed axon, Na^+ and K^+ channels were included with a density of $g_{Na} = 30{,}000$ and $g_{Kv} = 400$. We set AP threshold to -63 mV (Gulledge and Stuart, 2003). Synaptic inputs were simulated as conductances with 0.2 ms rise and 2 ms decay time constants and a reversal potential of 0 mV (Häusser and Roth, 1997). The nominal temperature was set to 35°C.

The conductance density of I_h (g_h) was distributed across compartments using the following exponential function: $g_h = y_0 + A \exp(d/\lambda)$, with $y_0 = -2$ pS/μm^{-2}, $A = 4.28$ pS/μm^{-2}, $\lambda = 323$ μm, and d is the distance from the soma. These values were obtained from an exponential fit to the experimental data in Figure 1*B* after correction for the 5.1-fold reduction in I_h conductance under physiological conditions in which the external potassium concentration is 2.5 mM (supplemental Fig. S2, available at www.jneurosci.org as supplemental material) and assuming a membrane area of 4.5 μm^2 at the pipette tip (Engel and Jonas, 2005). The corrected and scaled g_h implemented in NEURON gave rise to a range of I_h densities between 2.3 pS/μm^2 at the soma to 93 pS/μm^2 in the distal apical dendrites ~1000 μm from the soma and led to changes in V_m that were found experimentally (supplemental Fig. S1, available at www.jneurosci.org as supplemental material). The I_h reversal potential was set at -45 mV.

To investigate the impact of stochastic fluctuations attributable to probabilistic opening and closing of channels on AP output, we implemented stochastic channel gating in the NEURON-extension NMODL (Hines and Carnevale, 2000). For I_h, a simple two-state Hodgkin–Huxley scheme was used. In each segment, each closed single I_h channel had the chance to open within the iteration time, dt_{nrn}, with the probability, P_{open}:

$$P_{open} = \int_{t=0}^{dt_{nrn}} \alpha(v)\exp(-\alpha(v)t)dt = 1 - \exp(-\alpha(v)dt_{nrn}),$$

where $\alpha(v)$ is the rate of channel opening depending on the local membrane potential, v. Correspondingly, each open channel had the chance to close with P_{close} depending on the rate of channel closing, $\beta(v)$. The opening rate $\alpha(v)$ was defined by

$$\alpha(v) = \frac{A(v + B)}{\exp\left(\frac{v + B}{C} - 1\right)},$$

and the closing rate $\beta(v)$ was defined by

$$\beta(v) = D \exp(v/E).$$

This led to Hodgkin–Huxley-type channel kinetics with single exponential activation kinetics (power = 1) and no inactivation (Hodgkin and Huxley, 1952). The five free parameters, A, B, C, D, and E, were determined by simultaneously fitting $1/(\alpha(v) + \beta(v))$ to the voltage dependence of the time constant of I_h activation and deactivation and $\alpha(v)/(\alpha(v) + \beta(v))$ to the activation curve (see Fig. 6*A*). The sum of squared errors was minimized using the Levenberg–Marquardt method (Mathematica 4.1; Wolfram Research, Champaign, IL), with the time constants of activation and deactivation weighed with the inverse of the maximum value in the dataset, and the voltage activation curve weighed with 10 times the inverse of the maximum value in the dataset. The resulting parameters were $A = 6.43$ s^{-1}, $B = 154$ mV, $C = 11.9$ mV, $D = 193$ s^{-1}, and $E = 33.1$ mV and predicted the data adequately (see fits in Fig. 6*A*).

Stochastic Na^+ channels (see Fig. 7*E*,*F*) were modeled with a kinetic reaction scheme of eight states describing the m^3h Hodgkin–Huxley activation kinetics (Hille, 1978, 2001). As with stochastic I_h channels, each Na^+ channel had the chance to move to one of its neighboring states within the iteration time, dt_{nrn}, with the appropriate probability. The kinetic rate constants were based on previously published Na^+ channel models (see http://senselab.med.yale.edu/senselab/modeldb/).

For both stochastic I_h and Na^+ channels, the number of channels in each segment, was calculated from the current density and the surface area. For each iteration time point dt_{nrn}, the numbers of channels in the open and the closed state were stored, and the "macroscopic" I_h and Na^+ current were determined by summation of the appropriate number of single-channel events. Simulations were performed on three Intel Pentium processors 2.6 GHz, one 64-bit opteron AMD processor (2 × 1.6 GHz), and one Linux Cluster that contained 18 machines, each with two 2.6 GHz Intel Xeon central processing units housed in two IBM BladeCenters. The dt_{nrn} was set to 10 or 100 μs for simulations using stochastic I_h or 1 μs for simulations using stochastic Na^+ channels.

The power spectral density (PSD) of voltage (see Figs. 5, 6) was generated with Igor Pro from a 25 s sweep using the square-window method and fitted with a Lorentzian function, $S = A/(1 + (f/f_c)^2)$ (DeFelice, 1981). The predicted change in σ_V, when changing γ (see Fig. 6*D*), was based on theoretical work indicating that the variance of the macroscopic current, σ_I^2, is proportional to $\gamma^2 N$ (for an example, see Diba et al., 2004, their Eq. 15). Because the current density was the same in models with different single-channel conductance (i.e., γN = constant), σ_I^2 is proportional to γ. Thus, σ_I is proportional to $\sqrt{\gamma}$. The similarity between obtained and predicted voltage noise, $\sigma_{V,predicted}(\gamma) = \sigma_V(680\text{ fS})\sqrt{(\gamma/680\text{ fS})}$, indicates a linear relationship between σ_V and σ_I in our model.

Stochastic resonance was assessed during weak sinusoidal somatic current injection (I_{sin}) in the presence of direct current (DC) adjusted to be just suprathreshold (one AP per cycle) or just subthreshold (zero APs per cycle) in models with deterministic I_h channels. A binary output of AP timing was derived from the membrane voltage of the model (V_m), which was set to zero until V_m crossed 0 mV, and was then set to 1 for 1 ms (Stacey and Durand, 2000). The PSD of this binary output trace was determined using Igor Pro. The signal-to-noise ratio (SNR) ratio was defined as $(S - B)/B$, where S was the peak of the PSD at 3 Hz, and B was the average of the baseline noise of the PSD before and after 3 Hz. Stochastic resonance curves were fitted according to the theory of monostable systems with excitable dynamics and after deterministic "reinjection" to the resting state (Wiesenfeld et al., 1994):

$$\text{SNR} = \left(\frac{\varepsilon\,\Delta U}{D}\right)^2 e^{-(\Delta U/D)},$$

where ϵ is the signal strength, ΔU is a constant related to the threshold barrier height, and D is noise intensity. For D, the variance of the somatic membrane potential was used (Wiesenfeld et al., 1994), calculated from the fit to Figure 6*D*. The two free parameters ϵ and ΔU were fitted with nonlinear least-squares regression with Igor Pro.

Input/output curves (see Fig. 7*F*) were normalized, aligned to the synaptic conductance that generated APs with a probability of 0.5, and fitted with the sigmoid function $AP_{prob}(\Delta g) = (1 + \exp(-\Delta g/s))^{-1}$, where Δg is the change in synaptic conductance, and s represents the steepness of the AP probability curve.

Results

Cell-attached patch-clamp recordings were made from the apical dendrites of large layer 5 pyramidal neurons up to 900 μm from the soma, and I_h currents evoked by hyperpolarizing pulses from a holding potential 25 mV depolarized to the resting membrane potential (Fig. 1*A*). These currents could be blocked by 82 ± 7% ($n = 3$) by bath application of 50 μM of the I_h antagonist ZD 7288 (BoSmith et al., 1993; Robinson and Siegelbaum, 2003), indicating adequate specificity for I_h (Fig. 1*A*). To determine the dendritic distribution of I_h current, we plotted I_h current density against distance of the recording site from the soma (Fig. 1*B*). The distribution was well described by a single-exponential function (Fig. 1*B*), from which it can be inferred that I_h current density increases *e*-fold with every 325 μm. The time course of I_h current onset during 100 mV hyperpolarizing steps was best fit with a double-exponential function, with a τ_{fast} of 27.0 ± 1.5 ms and τ_{slow} of 155 ± 8 ms ($n = 88$). The ratio of the amplitude of the fast to slow time constants was 4.9 ± 0.3, indicating that fast activation kinetics dominate. The weighed single time constant of I_h activation was calculated to 49.7 ± 3.0 ms ($n = 88$). Steady-state voltage-activation curves were well described by a single Boltzmann function with a half-maximum activation (V_{half}) of, on average, −110 ± 1.5 mV and a slope constant of 10.1 ± 0.5 mV ($n = 9$) (Fig. 1*C*). At a few dendritic sites, cell-attached patch recordings were subsequently made with a saturating concentration of 8-Br-cAMP (100 μM, in the patch-pipette) to test for cyclic nucleotide modulation of I_h. On average, application of 8-Br-cAMP had no effect on the activation kinetics (τ_{fast} control, 22.0 ± 2.1 ms; cAMP, 21.4 ± 0.9 ms; paired *t* test, $p > 0.9$; $n = 10$) or the V_{half} (100 μM cAMP, −106 ± 0.9 mV; $n = 3$). These data are in good agreement with the relative insensitivity of the HCN1 isoform to cAMP regulation (Santoro and Tibbs, 1999) and an abundant expression of HCN1 in the layer 5 dendrites (Notomi and Shigemoto, 2004; Santoro et al., 2004).

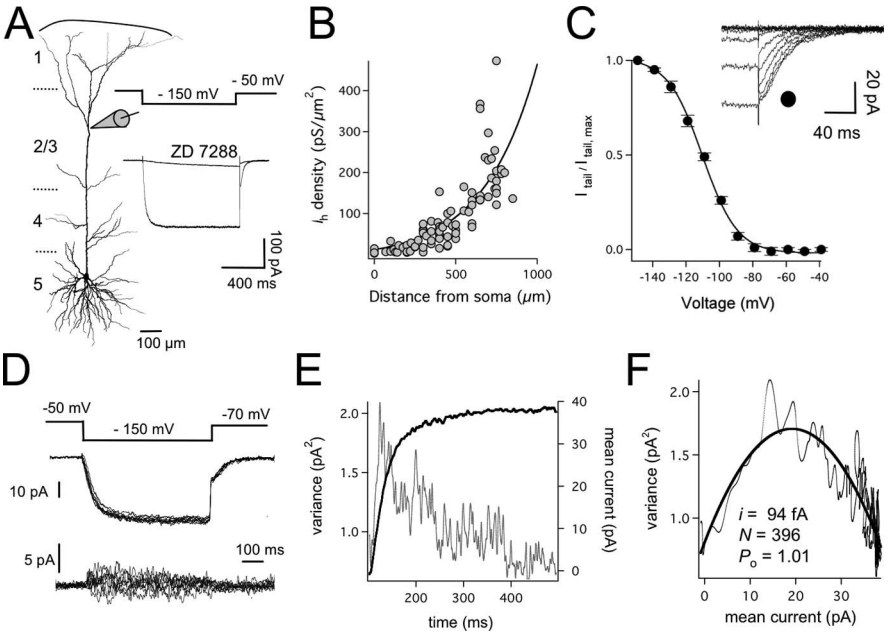

Figure 1. I_h current distribution, kinetics, and single-channel properties. ***A***, Schematic of the experimental setup during dendritic cell-attached recording 700 μm from the soma of a layer 5 pyramidal neuron (reconstructed from a biocytin fill). The different cortical layers are indicated. An example of I_h current evoked by a 100 mV hyperpolarizing pulse from a holding potential 25 mV depolarized from rest is shown before and after bath application of ZD 7288 (50 μM). ***B***, I_h current density plotted against distance from the soma ($n = 88$). Data fitted with a single-exponential function. ***C***, I_h voltage-activation curve generated from tail currents (inset) during hyperpolarizing steps between −40 and −150 mV ($n = 9$; 680 ± 21 μm from the soma). Data fitted with a Boltzmann function. ***D***, Superimposed successive single traces used for NSFA elicited by a 100 mV hyperpolarizing step (recorded 500 μm from the soma). Only 10 of 100 traces are shown. The corresponding subtracted differences from the 10 traces are given in the bottom panel. Currents were off-line digitally filtered at 100 Hz. ***E***, Fluctuation analysis of data in ***D***. Data of 100 successive sweeps were used to plot mean I_h current (black trace) and variance (gray trace) as a function of time. ***F***, Variance-mean plot for the data in ***E***. The data were well fitted by a parabola (black line) from which the single-channel amplitude *i*, the maximum number of channels *N*, and the open probability P_o were obtained.

Fluctuation analysis of I_h in cell-attached recordings

To examine the properties of single I_h channels, we used NSFA of macroscopic I_h currents (Conti et al., 1980; Sigworth, 1980; Alvarez et al., 2002). I_h currents in these experiments were activated by 400 ms hyperpolarizations to maximize the number of possible repetitions. Filtering of individual sweeps (Fig. 1*D*, top) was performed with a digital Gaussian filter at 100 Hz and the current variance (σ^2) calculated from the difference between 100 consecutive sweeps (Fig. 1*D*, bottom). The plot of the current σ^2 versus time had a peak coinciding with half-maximal activation at ~25 ms (Fig. 1*E*). Plots of the current σ^2 against mean I_h current amplitude could be well fit with a parabolic function, from which the single-channel amplitude (*i*), the total number of channels (*N*), and open probability (P_o) can be estimated (Fig. 1*F*). On average, at dendritic sites ~500 μm from the soma, NSFA gave estimates of *i* of 88 ± 9.9 fA, *N* of 342 ± 24, and P_o of 0.92 ± 0.03 ($n = 5$) during hyperpolarizing voltage steps of 100 mV from an estimated patch holding potential of approximately −50 mV.

Accuracy of parameters extracted using NSFA

How accurate are the values for *i*, *N*, and P_o obtained from NSFA? To assess this, we simulated I_h channels and performed NSFA on simulated macroscopic I_h currents. These simulations used I_h channels with activation kinetics similar to that observed experimentally (single exponential kinetics with τ of 50 ms). Two different channels were simulated, one without flicker (Fig. 2*A*, C–O) and one with channel flicker (Fig. 2*B*, C–C–O). In both cases, *i* was 100 fA and *N* was 500. In the case of the nonflickering channel, P_o was 1 (Fig. 2*A*), whereas P_o was 0.5 in the flickering channel (Fig. 2*B*, forward and backward rates, δ, into and out of the open state were equal). Simulated macroscopic I_h current traces were generated by adding 500 single-channel traces (Fig. 2*A*,*B*) and realistic recording noise. These currents were digitally filtered at frequencies ranging from 2 Hz to 10 kHz and subjected

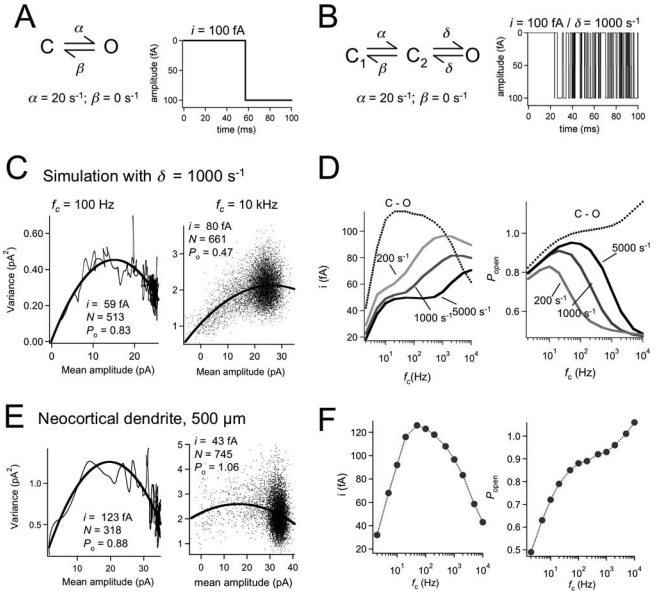

Figure 2. Accuracy of parameters extracted with NSFA. ***A***, I_h channels simulated with a simple gating model. The rate from the closed (C) to the open (O) state was set to be 20 s^{-1}, and P_o was set to 1. The right panel shows an example of a simulated single-channel trace with amplitude *i* of 100 fA. ***B***, Flickering I_h channels were simulated by adding an additional shut state C_2 to the scheme used in ***A***. The rate into and out of the open state, δ, was equal, leading to $P_o = 0.5$. The other channel rates are not changed. The right panel shows an example of a simulated single-channel trace with the flicker frequency δ set to 1000 s^{-1}. For clarity, only 100 ms of the 400 ms trace is shown. ***C***, Examples of variance-mean plots of simulated I_h channels with δ set to 1000 s^{-1} using a filter cutoff frequency, f_c, of 100 Hz (left) and 10 kHz (right). The parameters obtained from NSFA fitting (black lines) are indicated. ***D***, The influence of filtering on the parameters extracted with NSFA was investigated systematically by varying f_c from 2 Hz to 10 kHz. The lines represent simulations with different flickering frequencies (δ ranging from 200 to 5000 Hz). With increasing flickering frequency, higher cutoff frequencies are required to extract the correct parameters using NSFA. The dotted lines represent the parameters obtained with the nonflickering C–O model. ***E***, Variance-mean plots for experimental data recorded 500 μm from the soma and low-pass filtered at 100 Hz (left) or 10 kHz (right). The parameters obtained from NSFA are indicated. ***F***, The single-channel parameters *i*, *N*, and P_o are plotted versus f_c for the experimental data shown in ***E***. Note the high similarity to the nonflickering model (C–O) shown in ***D***.

to NSFA. An example of the effect of filtering on variance-mean plots for simulated I_h channels using a model with 1 kHz flicker is shown in Figure 2*C* after filtering at 100 Hz or 10 kHz. A full analysis of the impact of filtering on the parameters extracted with NSFA for the nonflickering and flickering models is shown in Figure 2*D*. These plots indicate that, in the nonflickering model, *i* is underestimated during filtering at less than ~20 Hz or more than ~1 kHz (Fig. 2*D*, left), leading to overestimations of *N* (data not shown), whereas P_o increased monotonically with filter cutoff frequency (Fig. 2*D*, right). These simulations suggest that, in a situation in which there is no channel flicker, the best estimates of single I_h channel parameters are obtained after filter at ~100 Hz. The situation was reversed in models with channel flicker, with the estimated value of *i* increasing monotonically with cutoff frequency (Fig. 2*D*, left), whereas P_o increased and then decreased with increasing cutoff frequency and only converged to its appropriate value (0.5) at the highest cutoff frequencies tested (Fig. 2*D*, right). Thus, under conditions of high-frequency channel flickering, NSFA will only be accurate when the cutoff frequency is set at or above 10 kHz.

With these theoretical relationships in mind, we tested the impact of filtering on the parameters extracted with NSFA for native I_h currents. Macroscopic I_h currents recorded at 10 kHz bandwidth were off-line digitally filtered at cutoff frequencies ranging from 2 Hz to 10 kHz. Variance-mean plots of recorded I_h currents after filtering at 100 Hz and 10 kHz are shown in Figure 2*E*. Figure 2*F* shows the estimated parameters obtained with NSFA for all cutoff frequencies tested. Similar to the nonflickering model, with increasing cutoff frequency *i* increased and then decreased, whereas P_o increased monotonically (similar results were observed in four other datasets). The impact of filtering on the single-channel parameters extract using NSFA of native I_h currents is therefore similar to that observed in the nonflickering model, suggesting that native I_h channels do not undergo significant flickering in the frequency range below ~ 5 kHz. Given this, these findings suggest that a cutoff filter frequency of ~100 Hz is optimal for obtaining the best estimates from NSFA. This is also consistent with theoretical work indicating that errors attributable to filtering will occur if the time constant of filtering (τ_{filter}) is more than 1/10 of the time constant of channel activation (Alvarez et al., 2002). In neocortical dendrites, I_h has a weighted time constant of activation of ~50 ms. Thus, in our case, τ_{filter} should not be >5 ms, corresponding to a low-pass cutoff frequency (f_c) of $1/(2\pi\tau_{filter})$ or ~30 Hz.

Finally, we investigated the accuracy of the parameters extracted with NSFA under a large range of different signal-to-noise conditions in our nonflickering model filtered at 100 Hz by varying *i* and *N* systematically (supplemental Fig. S3, available at www.jneurosci.org as supplemental material). From these simulations, we found that, if the amplitude of macroscopic I_h currents is <1 pA or *i* is <10 fA, the errors in *i*, *N*, and P_o are large (> 50%) and thus highly inaccurate. However, if the macroscopic I_h current is >10 pA, as typically found in this study, the errors are <20%. Together, these simulations indicate that NSFA has sufficient precision to accurately estimate the single-channel parameters of I_h channels under our recording conditions.

Dependence of I_h single-channel properties on voltage

Does NSFA of macroscopic I_h currents accurately describe the voltage-dependent properties of I_h? To address this, hyperpolarizing pulses of −100 and −60 mV amplitude were alternated at 1 s intervals, and NSFA was performed on the obtained variance-mean relationships (Fig. 3*A*) (six patches ~570 μm from the soma). Because the total channel number *N* cannot be estimated precisely when channels are not fully activated, we fixed *N* during fitting of variance-mean plots for −60 mV steps to the value estimated during NSFA of −100 mV steps in the same patch. From this analysis, P_o was estimated to be, on average, 0.94 ± 0.03 during −100 mV steps and 0.55 ± 0.05 during −60 mV steps ($n = 6$). These estimates of P_o follow a voltage dependence similar to that obtained for the I_h activation curve determined from tail currents (Fig. 3*B*). The unitary amplitude, *i*, was significantly smaller during −60 mV steps compared with −100 mV steps (Fig. 3*C*, left) ($p < 0.001$), as expected because of the reduced driving force, whereas the unitary conductance, γ, was not statistically different (Fig. 3*C*, right) ($p > 0.13$). In conclusion, the results above indicate that NSFA of macroscopic I_h currents accurately describes the voltage-dependent properties of single I_h channels.

Dependence of I_h single-channel properties on location

Previous studies on I_h in layer 5 pyramidal dendrites have reported a significantly higher current density at distal dendritic locations (Williams and Stuart, 2000; Berger et al., 2001). Because the macroscopic I_h current is determined by the product of *i*, *N*, and P_o, we can now separate which of these factors underlies the

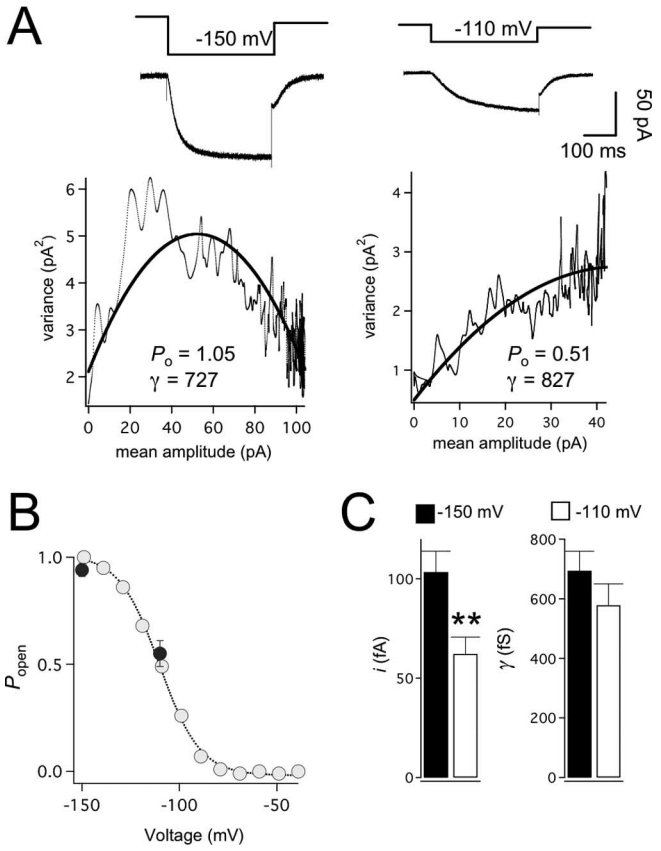

Figure 3. Voltage-dependent properties of I_h obtained with NSFA. ***A***, Top, I_h currents evoked by hyperpolarizing steps to −150 mV (left) and −110 mV (right). Bottom, Fitting variance versus mean of the plots (black line) yielded a P_o of 1.05 with 889 channels and *i* of 109 fA during steps to −150 (left), whereas P_o was reduced to 0.51 and *i* to 91 fA during steps to −110 mV (right). *N* was fixed to that obtained during steps to −150 mV (889) during fitting of the NSFA data for steps to −110 mV (black line). ***B***, Pooled data ($n = 5$) of P_o during steps to −150 mV (0.94 ± 0.03) and −110 mV (0.54 ± 0.05; filled circles) is consistent with the activation curves obtained from I_h tail-current amplitudes (open circles; same data as in Fig. 1*C*). ***C***, Histogram of single-channel current amplitude *i* (left) and conductance γ (right) extracted with NSFA during steps to −150 and −110 mV. $^{**}p < 0.001$ ($n = 6$).

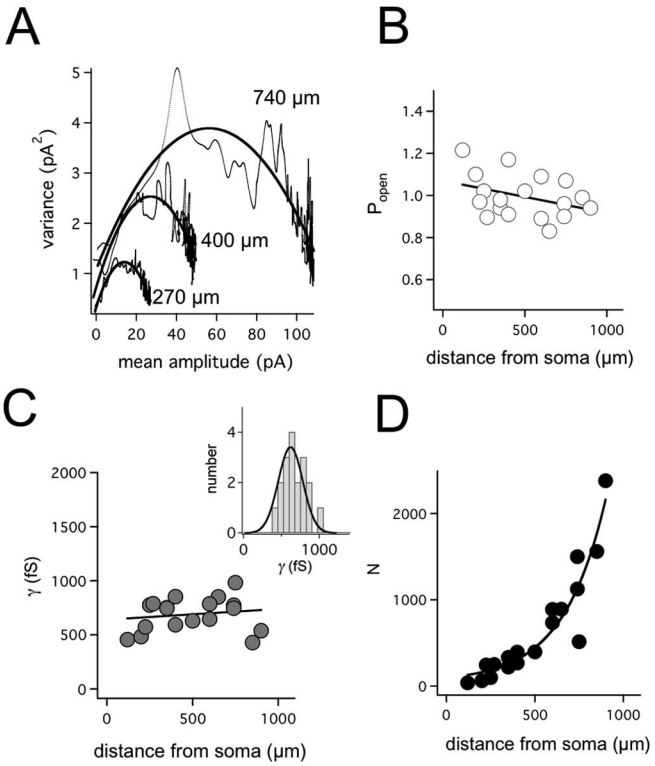

Figure 4. NSFA reveals a distance-dependent increase in *N*. ***A***, Superimposed examples of variance-mean plots for three dendritic locations (270, 400, and 740 µm from the soma) with the variance-mean fits (black lines). ***B***, Plot of open probability P_o versus recording distance from the soma. Data were fitted with a regression (slope of −0.015; $n = 18$). ***C***, Plot of single-channel conductance γ versus distance from the soma. Data fitted with a linear regression (slope of +0.11; $n = 18$). Inset shows a histogram of γ revealing a single population well fitted with a Gaussian function ($n = 18$). ***D***, Plot of the number of channels per patch (*N*) versus distance (*d*) from the soma. The data are well described by a single-exponential function of the form: $49 \times \exp(d/240) + 47$, indicating that the I_h channel number increases *e*-fold for a 240 µm change in distance.

highly nonuniform subcellular distribution of I_h in these neurons (Fig. 1*B*). Three examples of variance-mean plots obtained from recordings 270, 400, and 740 µm from the soma are shown in Figure 4*A*. Figure 4*B* shows that, when P_o is plotted as a function of recording location, for distances from ~120 to 900 µm from the soma, no clear dependence exists on dendritic site. Similarly, the I_h single-channel conductance, γ, was independent of the dendritic recording location (Fig. 4*C*). Plotting γ as a histogram indicates that γ represents a single population with average amplitude of 676 ± 35 fS (Fig. 4*C*, inset) ($n = 18$). In contrast, *N* was found to rise steeply with distance from the soma (Fig. 4*D*). An exponential fit to this data indicates that *N* increases *e*-fold for a 240 µm path length along the main apical dendrite of layer 5 pyramidal neurons, similar to the *e*-fold change in current density (Fig. 1*B*). At the most distal dendritic locations examined (900 µm from the soma), we observed as many as ~2500 I_h channels per dendritic patch, whereas at the most proximal sites (120 µm from the soma), as few as 40 channels per patch were observed. This gradient is essentially identical to the reported 60-fold increase in immunogold-labeled HCN1 particles in layer 5 dendritic membrane (Lorincz et al., 2002). These data correspond to I_h channel densities of 9–550/µm^2, assuming a membrane patch area of ~4.5 µm^2 (Engel and Jonas, 2005). The high density of I_h in the distal dendrites of layer 5 pyramidal neurons is comparable with the density of voltage-activated Na^+ channels found at nodes of Ranvier (Hille, 2001). In conclusion, these data indicate that the nonuniform scaling of I_h current density is generated by an exponential increase in channel number per dendritic membrane area, leading to high channel densities in distal dendrites.

Contribution of stochastic I_h channel gating to membrane noise

The results above indicate that I_h channels have a very small single-channel conductance yet can be expressed at very high densities. Why is the single-channel conductance of I_h so small? Clearly, it would be energetically more efficient to increase single-channel conductance, for example by 10-fold to 6.8 pS, thereby reducing channel number by a factor of 10 for the same current density. One possible explanation for the small single-channel conductance of I_h is that there are other constraints on the system, such as voltage noise. Previous work indicates that the stochastic opening and closing of voltage-dependent channels can generate fluctuations in membrane potential, which could be a significant source of voltage noise in excitable cells (DeFelice, 1981; White et al., 2000). To directly address whether the stochastic gating of single I_h channels contributes to membrane noise, we recorded voltage noise at the resting membrane potential in the

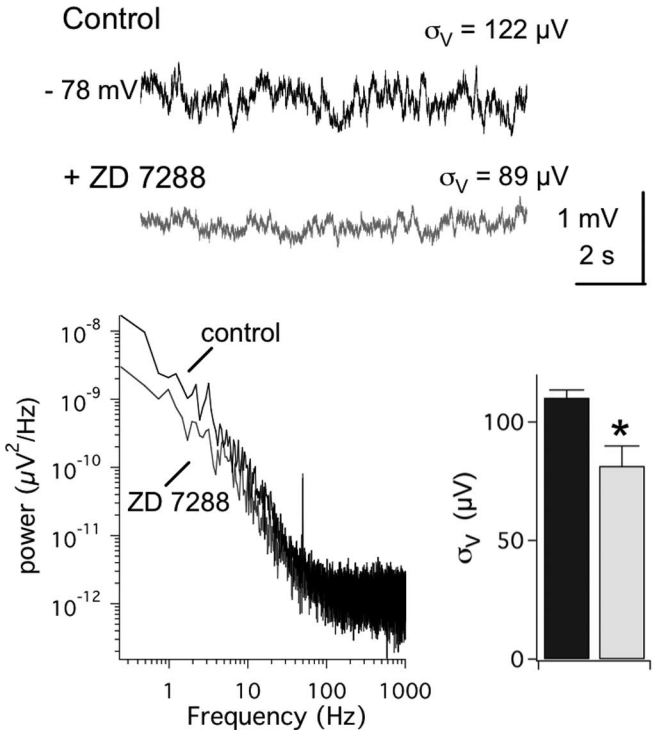

Figure 5. Impact of I_h channel gating on somatic voltage noise. Whole-cell somatic voltage recordings before (top trace; black) and after (bottom trace; gray) I_h channel block by bath application of ZD 7288 (50 μM). All data were recorded in the presence of synaptic blockers and TTX. DC injection was used to maintain the same membrane potential in control and ZD 7288. Left, Power spectrum of the same traces indicating that ZD 7288 attenuates voltage fluctuations in the low-frequency range. Right, Population data of the average SD, σ_V, of the somatic voltage noise in control (black bar) and ZD 7288 (gray bar).

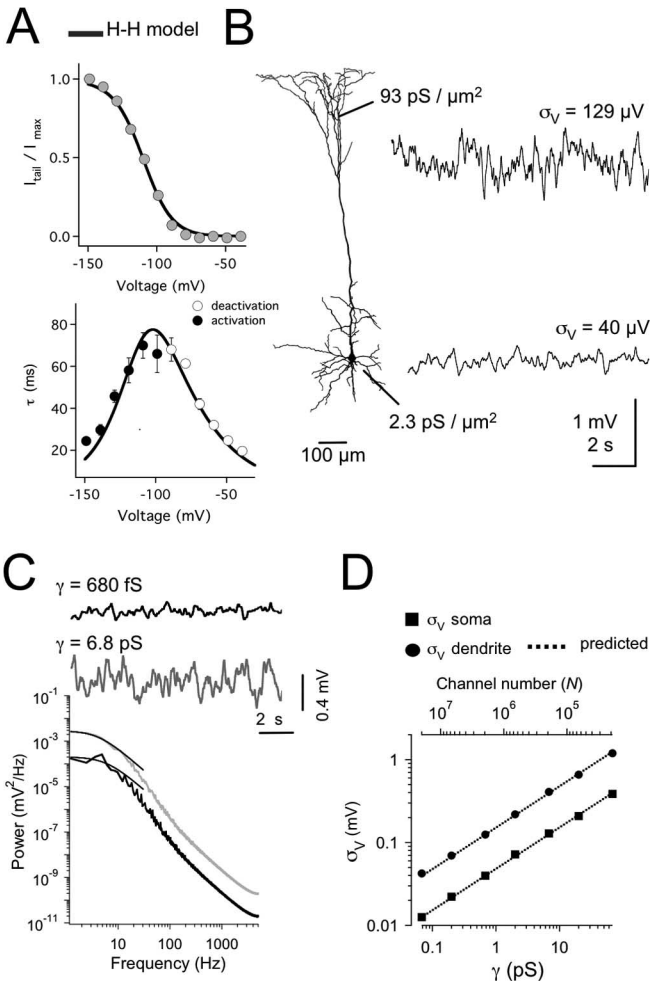

Figure 6. Impact of I_h channel single-channel conductance on voltage noise in a model. ***A***, Modeling of I_h kinetics using Hodgkin–Huxley (H–H) formalism. Steady-state voltage-activation curve (top) and the voltage dependence of activation (weighted single time constant; filled circles, bottom) and deactivation (open circles) together with the predictions from the Hodgkin–Huxley I_h model (lines). ***B***, Left, Morphology of the compartmental layer 5 neuron. Conductance densities at the soma and a distal dendritic location, together with representative examples (right) of the resting membrane potential at the soma (−79 mV; bottom trace) and distal dendrites (−63 mV; 1000 μm from the soma; top trace) using a model with single-channel conductance γ of 680 fS. ***C***, The power of somatic membrane potential fluctuations versus frequency for models with γ of 680 fS (black) and 6.8 pS (gray). Data fitted with a Lorentzian function (see Materials and Methods) from 1 to 30 Hz giving a cutoff frequency f_c of 6.0 and 4.2 Hz, respectively, in the models with γ of 680 fS and 6.8 pS. ***D***, The SD of the resting membrane potential σ_V plotted against γ and total N used in the simulations. The squares represent σ_V at the soma and the circles σ_V at a dendritic position 1000 μm from the soma. The lines are the predicted relationship between σ_V and γ (see Materials and Methods).

presence of blockers for NMDA, AMPA, $GABA_A$, and Na^+ channels. In Figure 5, an example is shown of control membrane potential fluctuations at the soma with an SD, σ_V, of 122 μV (Fig. 5, black trace). To isolate the contribution of I_h channels to these voltage fluctuations, we bath applied 50 μM ZD 7288 (BoSmith et al., 1993). This led to a hyperpolarization of the somatic resting membrane by 11 mV (average change, -10.3 ± 0.5 mV; $n = 6$), which was corrected for by positive DC injection to obtain a similar resting membrane potential as in control (−77.9 mV). Under these conditions, σ_V was reduced to 89 μV (Fig. 5, gray trace). Spectral analysis of traces before and after ZD 7288 showed that I_h noise is particularly dominant in the low-frequency range (Fig. 5, left). On average, application of ZD 7288 lead to a reduction of σ_V by 33 ± 7 μV (Fig. 5, right) ($n = 6$; paired t test, $p < 0.01$), showing that native I_h channels contribute significantly to voltage noise at resting membrane potentials.

Impact of I_h single-channel conductance on membrane noise

Next we investigated the impact of I_h single-channel properties on membrane voltage noise using a model in which single-channel conductance and number could be varied in a controlled manner. A stochastic Hodgkin–Huxley model of I_h based on our experimental data (Fig. 6*A*) was introduced into a morphologically realistic model of a layer 5 pyramidal neuron (Fig. 6*B*). The model contained voltage-activated Na^+, K^+, and Ca^{2+} conductances distributed uniformly throughout the dendritic tree, together with a stochastic I_h channel model distributed exponentially to mimic the experimentally observed increase in I_h current density with distance from the soma (Fig. 1*B*). Addition of I_h depolarized the soma by 10 to −79 mV and set the membrane potential in the very distal tuft branches to −65 mV. This effect of I_h on the resting membrane potential was quantitatively similar to experimentally observed changes in membrane potential with distance from the soma (supplemental Fig. S1, available at www.jneurosci.org as supplemental material).

We first performed simulations using I_h channels with a single-channel conductance of 680 fS, the experimentally determined value. Figure 6*B* shows that, using this model, small fluctuations in somatic membrane potential occur with a σ_V of 40 μV (Fig. 6*B*, bottom trace). As expected, because of the higher density of I_h in distal dendrites, as well as their small diameter, fluctuations in membrane potential at distal dendritic locations

(1000 μm from the soma) were significantly larger than at the soma, with σ_V being 129 μV (Fig. 6*B*, top trace). We next performed simulations with a single-channel conductance of 6.8 pS, 10-fold greater than observed experimentally while maintaining the same current density by scaling down *N*. Note that 6.8 pS is still in the low range compared with the single-channel conductance of most other ion channels (Hille, 2001). Increasing the I_h single-channel conductance, γ, to 6.8 pS increased σ_V to 129 μV at the soma (Fig. 6*C*, bottom, gray trace) and up to 408 μV in dendritic compartments ~1000 μm from the soma (data not shown). Analysis of the PSD of voltage fluctuations indicated that this increase in membrane noise was similar at all frequencies of the power spectrum (Fig. 6*C*). The cutoff frequency of the PSD was slightly lower at the soma than in the dendrites (~5 vs ~8 Hz), presumably because of greater "filtering" of voltage fluctuations at the soma by the larger somatic capacitance (data not shown).

To compare the voltage noise introduced by I_h with that generated by channel noise from voltage-activated Na^+ channels, we performed simulations using a stochastic Na^+ channel model with $\gamma_{Na} = 10$ pS. In these simulations, we used a deterministic I_h model to allow us to isolate the contribution of voltage-activated Na^+ channels to membrane noise independent of I_h channel noise. At resting membrane potentials, stochastic Na^+ channels generated membrane noise with $\sigma_V = 7.3$ μV at the soma, significantly smaller than the observed $\sigma_V = 40$ μV in models with stochastic I_h channel ($\gamma = 680$ fS). In dendritic compartments ~1000 μm from the soma, σ_V increased to 47 μV (compared with 129 μV for I_h channels). These data indicate that, at resting membrane potentials, the voltage noise attributable to stochastic gating of I_h channels is significantly larger than that mediated by Na^+ channels.

Despite the uniform dendritic Na^+ channel density in the model, the Na^+ channel voltage noise was greatest at distal dendritic locations. Given recent experimental evidence that Na^+ channel noise is greater at depolarized potentials (Jacobson et al., 2005), we reasoned that the larger membrane fluctuations at distal dendritic locations were generated by increased activation of voltage-dependent Na^+ channels as a consequence of the depolarizing action of nonuniform I_h (supplemental Fig. S1, available at www.jneurosci.org as supplemental material). Consistent with this idea, when the I_h density in our model was set to be low and uniform, leading to a homogeneous resting potential of −83 mV, the σ_V of Na^+ channel-induced membrane noise was 2.7 μV in both distal dendritic and somatic compartments. This suggests a dual role for I_h on membrane noise in the distal dendrites: increasing membrane noise via the high density of distal dendritic I_h channels, as well as via depolarization-induced activation of dendritic Na^+ channels.

The relationship between γ, *N*, and σ_V is depicted in a log–log plot in Figure 6*D*. Previous theoretical work indicates that the current variance, σ_I^2, is proportional to *N* and the square of γ (White et al., 2000; Diba et al., 2004). Consistent with this idea, the observed change in σ_V was well predicted by the expected change in current noise, with σ_V proportional to the square root of γ (Fig. 6*D*). These simulations indicate that the impact of I_h single-channel conductance on voltage noise follows known theoretical descriptions of the contribution of single-channel properties to current noise. From this, it follows that, for a given current density, reducing I_h single-channel conductance, rather than channel number, is the most effective means to reduce the impact of stochastic gating of I_h on membrane noise.

Impact of I_h channel noise on action potential fidelity

To assess the functional implications of I_h channel noise, we first analyzed the probability and timing of AP generation in response to weak periodic suprathreshold inputs. A small sinusoidal current (3 Hz; 4 pA peak-to-peak) was injected into the soma together with a larger DC adjusted to elicit one AP per sine-wave cycle in models with deterministic I_h. These current injections elicited, on average, one AP per sine-wave cycle in models with stochastic I_h with a single-channel conductance, γ, of 680 fS (Fig. 7*A*). The ability to detect the sinusoidal signal (the SNR) was quantified from the 3 Hz peak in the PSD (see Materials and Methods). The temporal precision of AP output was quantified from the SD of the temporal jitter in AP timing (σ_t) (Fig. 7*A*). Increasing γ 10-fold to 6.8 pS led to an increase in AP failures and spontaneous APs not phase locked to the peak of the weak input signal (Fig. 7*B*), leading to a decrease in both the SNR (Fig. 7*C*, black diamonds) and temporal precision (Fig. 7*C*, blue diamonds). Systematic variation of γ between 0.4 and 400 pS showed that, as γ increases, there is an ~100-fold decrease in SNR and a qualitatively similar decrease in temporal precision (Fig. 7*C*, diamonds).

Can the detection of subthreshold periodic signals, however, be facilitated by membrane noise via stochastic resonance (Wiesenfeld et al., 1994; Wiesenfeld and Moss, 1995; Stacey and Durand, 2000)? To examine the impact of I_h channel noise on stochastic resonance, the amplitude of DC injected into the soma was adjusted so that small sinusoidal currents (3 Hz; 4 pA peak-to-peak) were just subthreshold in models with deterministic I_h. In models with stochastic I_h, these current injections elicited stochastic resonance, with the SNR dependent on the amplitude of the I_h single-channel conductance, γ (Fig. 7*C*). In the example shown in Figure 7*C* (red circles), the SNR peaked in I_h models in which γ was ~10 pS. According to classical stochastic resonance theory (Wiesenfeld and Moss, 1995), the SNR peak is expected at half of the threshold barrier height (ΔU). Consistent with this expectation, reducing ΔU by using larger DCs, which brings subthreshold sinusoidal currents closer to AP threshold, led to SNR peaks at smaller values of γ (e.g., <1 pS; data not shown). Decreasing the amplitude of sinusoidal currents from 4 to 1 pA with identical values of ΔU resulted in SNR peaks at approximately the same value of γ but smaller SNR amplitude. These findings indicate that, although detection of small periodic signals can be improved by voltage noise from stochastic gating of I_h channels, the optimal I_h single-channel conductance critically depends on the characteristics of the signal that is to be detected.

We also investigated the impact of I_h channel noise on AP output during EPSPs of varying amplitude located 400 μm from the soma (Fig. 7*D–F*). For all EPSP amplitudes, ~25 trials were repeated while changing only the values for the random number generator used to generate stochastic gating of simulated I_h channels. In models with γ of 680 fS, the variance in spike timing was small ($\sigma_t \leq 1$ ms), and the precision ($1/\sigma_t$) increased linearly with synaptic strength (Fig. 7*E*, black diamonds). In comparison, considerable more jittering in AP latency was observed in models with γ of 6.8 pS, and precision increased only weakly with EPSP amplitude (Fig. 7*E*, blue circles). Simulations with stochastic Na^+ channels, but deterministic I_h channels, indicated that stochastic gating of Na^+ channels introduces similar reductions in temporal precision to that seen in models with stochastic I_h with γ of 6.8 pS (Fig. 7*E*, open circles).

The reduced precision of AP generation in models with larger I_h channel noise was associated with a shallower slope of the input–output relationship of EPSP amplitude versus the proba-

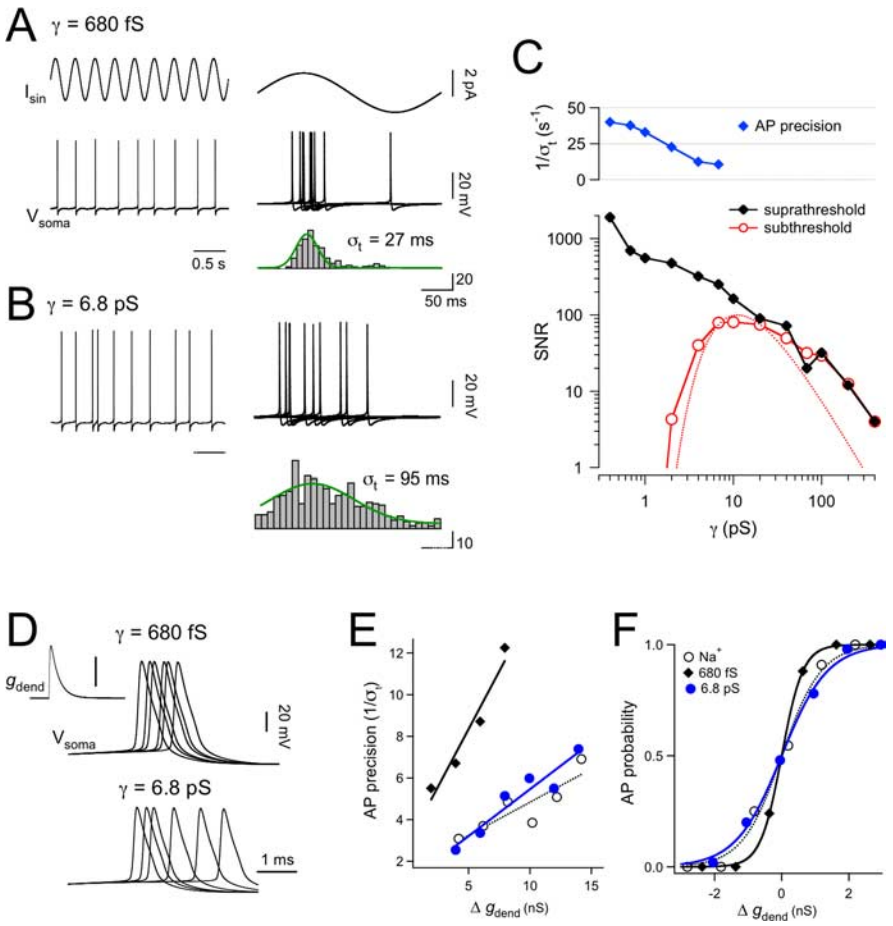

Figure 7. Impact of I_h single-channel noise on the fidelity of AP output in the model. ***A***, Somatic injection of a small suprathreshold sinusoidal current signal (I_{sin} = 4 pA; 3 Hz; top trace) elicited, on average, one AP per sine-wave cycle (bottom trace) in a model with γ of 680 fS. Right, Superimposed responses on an expanded time scale. Bottom, Histogram of AP onset latency relative to the phase of the sine wave for 400 consecutive sine-wave cycles. Data were fitted with a Gaussian function (green line) with SD σ_t. ***B***, Corresponding plots as in ***A*** but with increased γ to 6.8 pS. Note the threefold increase in AP jitter. ***C***, SNR determined from the 3 Hz peak in the power-spectrum density, and temporal precision (blue diamonds, $1/\sigma_t$) are plotted as a function of γ (range, 0.4–400 pS). Subthreshold sinusoidal current injections (red; I_{sin} = 4 pA) and suprathreshold injections (black; I_{sin} = 4 pA) were analyzed for stochastic resonance. The dotted lines are fits according to stochastic resonance theory (see Materials and Methods). ***D***, Superimposed sweeps of APs evoked by a simulated excitatory synaptic conductance (g_{dend}; left trace; calibration bar, 60 nS) injected 400 μm from the soma in models with single-channel conductance γ of 680 fS (top) and 6.8 pS (bottom). Note the larger trial-to-trial variability (jittering) in models with large γ. ***E***, Spike precision defined as $1/\sigma$ and plotted versus the change in amplitude of the excitatory synaptic conductance in models with γ of 680 fS (black diamonds) and 6.8 pS (blue circles). For comparison, a model with deterministic I_h and stochastic Na^+ channels with γ_{Na} = 10 pS is shown (open circles). ***F***, Input–output relationship showing the probability of AP generation versus the change in amplitude of the excitatory synaptic conductance in models with γ = 680 fS (black line; steepness of the sigmoid fit, s = 0.31 nS) and γ = 6.8 pS (blue line; s = 0.68 nS). For comparison, a model with deterministic I_h and stochastic Na^+ channels with γ_{Na} = 10 pS is shown (open circles; s = 0.59 nS).

bility of AP generation (Fig. 7*F*). A change in slope of this input–output function indicates that models with higher I_h single-channel conductance have a larger threshold uncertainty (White et al., 2000). Simulations with stochastic Na^+ channels but deterministic I_h channels also showed a larger threshold uncertainty (Fig. 7*F*, open circles). Note that the change in the input–output function during EPSPs in models with stochastic I_h did not translate into a change in slope of the AP firing frequency (f) versus input current (I) relationship (f/I curve) during long (1 s) pulses (data not shown). This was presumably the case because the level of background noise generated by stochastic gating of I_h (SD < 1 mV) was too small to cause a change in f/I gain, as observed by others during balanced synaptic noise (Chance et al., 2002).

Discussion

Using NSFA of native I_h currents combined with simulations of their biophysical properties, we provide, to our knowledge, the first estimation of the single-channel properties of I_h channels in the brain *in situ*. To explore the precision of NSFA, we analyzed simulated I_h currents with predetermined single-channel properties and studied the impact of filtering, indicating a high stability of the extracted single-channel parameters, as well as little if any channel flicker. Indeed, the observed unitary conductance of I_h of 680 fS is in good agreement with the previous estimate of 980 fS for I_f in the sinoatrial node of the heart (DiFrancesco, 1986). We go on to show both experimentally and in simulations that stochastic openings of I_h generate voltage noise, which impacts on the fidelity of action potential output.

Comparisons with previous studies

Although our data provide compelling evidence for small-conducting I_h channels, a recent study in acutely dissociated CA1 pyramidal neurons using excised patches from the soma has proposed a >10-fold higher single-channel conductance of 10 pS (Simeone et al., 2005). Such large single-channel openings (~1 pA), however, were not observed in previous cell-attached studies of native I_h currents in CA1 pyramidal neurons (Magee, 1998). In addition, it is also unclear how I_h currents were observed at all in the study of Simeone et al. (2005), given the evidence that I_h is very sensitive to enzymatic procedures for acute dissociation (Budde et al., 1994). Our findings in brain slices are also at odds with estimates of HCN single-channel conductance based on heterologously expressed HCN subunits (2.5–35 pS) (Johnson and Zagotta, 2005; Michels et al., 2005). Although the explanation for these discrepancies are also unclear, a number of proteins are known to interact with HCN subunits, such as Filamin A or TRIP8b (Gravante et al., 2004; Santoro et al., 2004). Additional experiments will be needed to address whether interaction of these proteins with HCN channels leads to modification of channel properties, such as single-channel conductance. Given this possibility, it is worth noting that the studies that used cell-attached recording configuration (the present study) (DiFrancesco, 1986) consistently observed a small single-channel conductance <1 pS. This may suggest that excised patch-clamp recordings disturb the single-channel properties of I_h, perhaps via removal of accessory or loss of interactions between HCN channels and critical cytosolic proteins.

I_h channel noise

Given the wide spectrum of observed unitary conductances for voltage-dependent channels (from ~1 to 300 pS) (Hille, 2001),

we asked why is the single-channel conductance of I_h so small? A growing number of studies indicate that noise generated by random channel opening limits neuronal response reliability (Schneidman et al., 1998; White et al., 2000), influences the energy efficiency of channels (Schreiber et al., 2002), and constrains the physical dimensions of axon diameters (Faisal et al., 2005). Conversely, noise can have a beneficial role by enhancing the detection of weak periodic signals via a stochastic resonance mechanism (Wiesenfeld and Moss, 1995) or via enhancing subthreshold oscillations (Dorval and White, 2005). Based on these studies, it seems likely that the magnitude of channel noise is under evolutionary pressure in biological systems seeking energy-efficient coding systems (Laughlin and Sejnowski, 2003). We show here that native I_h channels generate between ~40 and 130 μV of voltage noise (rms) spatially distributed from the soma to distal dendrites, with most of the power below 10 Hz (Figs. 5, 6). Although most recent studies have focused on the role of stochastic openings of Na^+ channels (Schneidman et al., 1998; Diba et al., 2004; Dorval and White, 2005; Faisal et al., 2005; Jacobson et al., 2005), we propose that I_h is also likely to be an important source of intrinsic channel noise in neurons. This would be expected to be the case for a number of reasons. First, channel noise is greater for voltage-dependent channels, like I_h, that have slow activation kinetics (Diba et al., 2004). Second, channel noise increases linearly with channel number (Diba et al., 2004), and, as we show, I_h channel densities can be very high, particularly at distal dendritic locations (Fig. 4). Third, channel noise would be expected to lead to larger voltage noise in smaller compartments in which I_h channel densities are maximal. Finally, the depolarizing gradient generated by I_h will enhance Na^+ channel noise. These observations indicate that the dynamic interplay between I_h and Na^+ channel noise will need to be considered in future studies investigating the impact of membrane noise in neuronal computation.

Functional implications of I_h channel gating on action potential output

We asked whether I_h noise is large enough to impact on AP output. This was shown to be the case both for perithreshold weak periodic stimuli and single EPSPs (Fig. 7). In models with high I_h single-channel conductance (6.8 pS), larger AP jitter and lower phase reliability were observed compared with models with the experimentally observed I_h single-channel conductance of 680 fS. In contrast to these negative aspects of I_h noise, models with stochastic I_h also showed stochastic resonance for very weak (1–4 pA) oscillatory inputs. Whether such noise-enhanced signal detection is functionally relevant in cortical layer 5 pyramidal neurons is presently unclear, because, under *in vivo* conditions, it seems likely that voltage noise will be dominated by the large fluctuations of ongoing, spatially distributed, synaptic activity at dendritic sites (Destexhe et al., 2003). Furthermore, although I_h noise could improve detection of weak sinusoidal signals, the optimal single-channel conductance was critically dependent on the characteristics of the input signal to be detected. Thus, it seems unlikely that stochastic resonance mechanisms have worked as a selection factor for I_h single-channel conductance. Rather, our results suggest that such selection, favoring small-conducting I_h channels, is more likely to depend on the influence of stochastic channel noise on the reliability of spike timing (Fig. 7*C*, top, *E*, *F*).

Although our studies concentrate on cortical layer 5 pyramidal neurons, which express I_h channels primarily in their dendrites, many of the results can be generalized in other neuronal and cell types. For example, expression of I_h in small-diameter compartments such as axons (Notomi and Shigemoto, 2004) would be expected to increase channel noise and limit the axonal conduction reliability (Faisal et al., 2005). In addition, because the magnitude of channel noise is further increased by slower channel activation kinetics (Diba et al., 2004), it seems likely that spike-time jitter will be even greater in cells in which HCN activation is slower, such as in the cardiac cells (DiFrancesco, 1984) and thalamic relay neurons (McCormick and Pape, 1990). Such predictions remain to be tested.

Given that theoretical relationships indicate that current noise is linearly dependent on single-channel number but changes with the square root of channel conductance (White et al., 2000; Diba et al., 2004), reducing single-channel conductance is an efficient means to reduce membrane noise attributable to stochastic channel gating. This result may well explain the small single-channel conductance of I_h channels in the brain and suggests that the single-channel conductance of I_h is evolutionarily constrained to be small to reduce its impact on both membrane noise and AP output.

In conclusion, our results indicate that native I_h channels in the brain have a small single-channel conductance, comparable in size with the single-channel conductance of I_f in the heart, which is likely to be critical for reducing membrane noise attributable to stochastic gating, thereby maintaining the fidelity of temporal patterns of AP output.

References

Alvarez O, Gonzalez C, Latorre R (2002) Counting channels: a tutorial guide on ion channel fluctuation analysis. Adv Physiol Educ 26:327–341.

Berger T, Larkum ME, Luscher H-R (2001) High Ih channel density in the distal apical dendrite of layer V pyramidal cells increases bidirectional attenuation of EPSPs. J Neurophysiol 85:855–868.

Biel M, Schneider A, Wahl C (2002) Cardiac HCN channels: structure, function, and modulation. Trends Cardiovasc Med 12:206–212.

BoSmith RE, Briggs I, Sturgess NC (1993) Inhibitory actions of ZENECA ZD7288 on whole-cell hyperpolarization activated inward current (If) in guinea-pig dissociated sinoatrial node cells. Br J Pharmacol 110:343–349.

Brown HF, DiFrancesco D, Noble SJ (1979) How does adrenaline accelerate the heart? Nature 280:235–236.

Budde T, White JA, Kay AR (1994) Hyperpolarization-activated Na^+-K^+ current (Ih) in neocortical neurons is blocked by external proteolysis and internal TEA. J Neurophysiol 72:2737–2742.

Chance FS, Abbott LF, Reyes AD (2002) Gain modulation from background synaptic input. Neuron 35:773–782.

Colquhoun D, Hatton CJ, Hawkes AG (2003) The quality of maximum likelihood estimates of ion channel rate constants. J Physiol (Lond) 547:699–728.

Conti F, Neumcke B, Nonner W, Stämpfli R (1980) Conductance fluctuations from the inactivation process of sodium channels in myelinated nerve fibres. J Physiol (Lond) 308:217–239.

DeFelice LJ (1981) Introduction to membrane noise. New York: Plenum.

Destexhe A, Rudolph M, Pare D (2003) The high-conductance state of neocortical neurons in vivo. Nat Rev Neurosci 4:739–751.

Diba K, Lester HA, Koch C (2004) Intrinsic noise in cultured hippocampal neurons: experiment and modeling. J Neurosci 24:9723–9733.

DiFrancesco D (1984) Characterization of the pace-maker current kinetics in calf Purkinje fibres. J Physiol (Lond) 348:341–367.

DiFrancesco D (1986) Characterization of single pacemaker channels in cardiac sino-atrial node cells. Nature 324:470–473.

Dorval Jr AD, White JA (2005) Channel noise is essential for perithreshold oscillations in entorhinal stellate neurons. J Neurosci 25:10025–10028.

Engel D, Jonas P (2005) Presynaptic action potential amplification by voltage-gated Na^+ channels in hippocampal mossy fiber boutons. Neuron 45:405–417.

Faisal AA, White JA, Laughlin SB (2005) Ion-channel noise places limits on the miniaturization of the brain's wiring. Curr Biol 15:1143–1149.

Gravante B, Barbuti A, Milanesi R, Zappi I, Viscomi C, DiFrancesco D

(2004) Interaction of the pacemaker channel HCN1 with filamin A. J Biol Chem 279:43847–43853.
Gulledge AT, Stuart GJ (2003) Excitatory actions of GABA in the cortex. Neuron 37:299–309.
Halliwell JV, Adams PR (1982) Voltage-clamp analysis of muscarinic excitation in hippocampal neurons. Brain Res 250:71–92.
Häusser M, Roth A (1997) Estimating the time course of the excitatory synaptic conductance in neocortical pyramidal cells using a novel voltage jump method. J Neurosci 17:7606–7625.
Hestrin S (1987) The properties and function of inward rectification in rod photoreceptors of the tiger salamander. J Physiol (Lond) 390:319–333.
Hille B (1978) Ionic channels in excitable membranes. Current problems and biophysical approaches. Biophys J 22:283–294.
Hille B (2001) Ion channels of excitable membranes, Ed 3. Sunderland, MA: Sinauer.
Hines ML, Carnevale NT (2000) Expanding NEURON's repertoire of mechanisms with NMODL. Neural Comput 12:995–1007.
Hodgkin AL, Huxley AF (1952) A quantitative description of membrane current and its application to conduction and excitation in nerve. J Physiol (Lond) 117:500–544.
Jacobson GA, Diba K, Yaron-Jakoubovitch A, Oz Y, Koch C, Segev I, Yarom Y (2005) Subthreshold voltage noise of rat neocortical pyramidal neurones. J Physiol (Lond) 564:145–160.
Johnson Jr JP, Zagotta WN (2005) The carboxyl-terminal region of cyclic nucleotide-modulated channels is a gating ring, not a permeation path. Proc Natl Acad Sci USA 102:2742–2747.
Laughlin SB, Sejnowski TJ (2003) Communication in neuronal networks. Science 301:1870–1874.
Lorincz A, Notomi T, Tamas G, Shigemoto R, Nusser Z (2002) Polarized and compartment-dependent distribution of HCN1 in pyramidal cell dendrites. Nat Neurosci 5:1185–1193.
Ludwig A, Zong X, Jeglitsch M, Hofmann F, Biel M (1998) A family of hyperpolarization-activated mammalian cation channels. Nature 393:587–591.
Magee JC (1998) Dendritic hyperpolarization-activated currents modify the integrative properties of hippocampal CA1 pyramidal neurons. J Neurosci 18:7613–7624.
McCormick DA, Pape HC (1990) Properties of a hyperpolarization-activated cation current and its role in rhythmic oscillation in thalamic relay neurones. J Physiol (Lond) 431:291–318.
Michels G, Er F, Khan I, Südkamp M, Herzig S, Hoppe UC (2005) Single-channel properties support a potential contribution of hyperpolarization-activated cyclic nucleotide-gated channels and If to cardiac arrhythmias. Circulation 111:399–404.
Notomi T, Shigemoto R (2004) Immunohistochemical localization of Ih channel subunits, HCN1–4, in the rat brain. J Comp Neurol 471:241–276.
Press WH (2002) Numerical recipes in C++: the art of scientific computing, Ed 2. Cambridge, UK: Cambridge UP.
Robinson RB, Siegelbaum SA (2003) Hyperpolarization-activated cation currents: from molecules to physiological function. Annu Rev Physiol 65:453–480.
Santoro B, Tibbs GR (1999) The HCN gene family: molecular basis of the hyperpolarization-activated pacemaker channels. Ann NY Acad Sci 868:741–764.
Santoro B, Liu DT, Yao H, Bartsch D, Kandel ER, Siegelbaum SA, Tibbs GR (1998) Identification of a gene encoding a hyperpolarization-activated pacemaker channel of brain. Cell 93:717–729.
Santoro B, Wainger BJ, Siegelbaum SA (2004) Regulation of HCN channel surface expression by a novel C-terminal protein–protein interaction. J Neurosci 24:10750–10762.
Schaefer AT, Larkum ME, Sakmann B, Roth A (2003) Coincidence detection in pyramidal neurons is tuned by their dendritic branching pattern. J Neurophysiol 89:3143–3154.
Schneidman E, Freedman B, Segev I (1998) Ion channel stochasticity may be critical in determining the reliability and precision of spike timing. Neural Comput 10:1679–1703.
Schreiber S, Machens CK, Herz AV, Laughlin SB (2002) Energy-efficient coding with discrete stochastic events. Neural Comput 14:1323–1346.
Sigworth FJ (1980) The variance of sodium current fluctuations at the node of Ranvier. J Physiol (Lond) 307:97–129.
Simeone TA, Rho JM, Baram TZ (2005) Single channel properties of hyperpolarization-activated cation currents in acutely dissociated rat hippocampal neurons. J Physiol (Lond) 568:371–380.
Stacey WC, Durand DM (2000) Stochastic resonance improves signal detection in hippocampal CA1 neurons. J Neurophysiol 83:1394–1402.
Stuart G, Spruston N (1998) Determinants of voltage attenuation in neocortical pyramidal neuron dendrites. J Neurosci 18:3501–3510.
Stuart GJ, Sakmann B (1994) Active propagation of somatic action potentials into neocortical pyramidal cell dendrites. Nature 367:69–72.
Wainger BJ, DeGennaro M, Santoro B, Siegelbaum SA, Tibbs GR (2001) Molecular mechanism of cAMP modulation of HCN pacemaker channels. Nature 411:805–810.
White JA, Rubinstein JT, Kay AR (2000) Channel noise in neurons. Trends Neurosci 23:131–137.
Wiesenfeld K, Moss F (1995) Stochastic resonance and the benefits of noise: from ice ages to crayfish and SQUIDs. Nature 373:33–36.
Wiesenfeld K, Pierson D, Pantazelou E, Dames C, Moss F (1994) Stochastic resonance on a circle. Phys Rev Lett 72:2125–2129.
Williams SR, Stuart GJ (2000) Site independence of EPSP time course is mediated by dendritic Ih in neocortical pyramidal neurons. J Neurophysiol 83:3177–3182.
Williams SR, Stuart GJ (2003) Voltage- and site-dependent control of the somatic impact of dendritic IPSPs. J Neurosci 23:7358–7367.
Zagotta WN, Olivier NB, Black KD, Young EC, Olson R, Gouaux E (2003) Structural basis for modulation and agonist specificity of HCN pacemaker channels. Nature 425:200–205.